

MVQ: Towards Efficient DNN Compression and Acceleration with Masked Vector Quantization

Shuaiting Li*
list@zju.edu.cn
Zhejiang University
Hangzhou, Zhejiang, China

Chengxuan Wang*
wangchengxuan@zju.edu.cn
Zhejiang University
Hangzhou, Zhejiang, China

Juncan Deng
dengjuncan@zju.edu.cn
Zhejiang University
Hangzhou, Zhejiang, China

Zeyu Wang
wangzeyu2020@zju.edu.cn
Zhejiang University
Hangzhou, Zhejiang, China

Zewen Ye
lucas.zw.ye@zju.edu.cn
Zhejiang University
Hangzhou, Zhejiang, China

Zongsheng Wang
wangzongsheng@zju.edu.cn
Zhejiang University
Hangzhou, Zhejiang, China

Haibin Shen
shen_hb@zju.edu.cn
Zhejiang University
Hangzhou, Zhejiang, China

Kejie Huang[†]
huangkejie@zju.edu.cn
Zhejiang University
Hangzhou, Zhejiang, China

Abstract

Vector quantization(VQ) is a hardware-friendly DNN compression method that can reduce the storage cost and weight-loading datawidth of hardware accelerators. However, conventional VQ techniques lead to significant accuracy loss because the important weights are not well preserved. To tackle this problem, a novel approach called MVQ is proposed, which aims at better approximating important weights with a limited number of codewords. At the algorithm level, our approach removes the less important weights through N:M pruning and then minimizes the vector clustering error between the remaining weights and codewords by the masked k-means algorithm. Only distances between the unpruned weights and the codewords are computed, which are then used to update the codewords. At the architecture level, our accelerator implements vector quantization on an EWS (Enhanced weight stationary) CNN accelerator and proposes a sparse systolic array design to maximize the benefits brought by masked vector quantization.

*Both authors contributed equally to this research.

[†]Corresponding author.

Permission to make digital or hard copies of all or part of this work for personal or classroom use is granted without fee provided that copies are not made or distributed for profit or commercial advantage and that copies bear this notice and the full citation on the first page. Copyrights for components of this work owned by others than the author(s) must be honored. Abstracting with credit is permitted. To copy otherwise, or republish, to post on servers or to redistribute to lists, requires prior specific permission and/or a fee. Request permissions from permissions@acm.org. *ASPLOS '25, March 30–April 3, 2025, Rotterdam, Netherlands*

© 2025 Copyright held by the owner/author(s). Publication rights licensed to ACM.

ACM ISBN 979-8-4007-0698-1/25/03...\$15.00

<https://doi.org/10.1145/3669940.3707268>

Our algorithm is validated on various models for image classification, object detection, and segmentation tasks. Experimental results demonstrate that MVQ not only outperforms conventional vector quantization methods at comparable compression ratios but also reduces FLOPs. Under ASIC evaluation, our MVQ accelerator boosts energy efficiency by 2.3× and reduces the size of the systolic array by 55% when compared with the base EWS accelerator. Compared to the previous sparse accelerators, MVQ achieves 1.73× higher energy efficiency.

CCS Concepts: • Computer systems organization → Systolic arrays; • Computing methodologies → Computer vision; • Hardware → Hardware-software codesign.

Keywords: neural networks; vector quantization; pruning; systolic arrays

ACM Reference Format:

Shuaiting Li, Chengxuan Wang, Juncan Deng, Zeyu Wang, Zewen Ye, Zongsheng Wang, Haibin Shen, and Kejie Huang. 2025. MVQ: Towards Efficient DNN Compression and Acceleration with Masked Vector Quantization. In *Proceedings of the 30th ACM International Conference on Architectural Support for Programming Languages and Operating Systems, Volume 1 (ASPLOS '25), March 30–April 3, 2025, Rotterdam, Netherlands*. ACM, New York, NY, USA, 15 pages. <https://doi.org/10.1145/3669940.3707268>

1 Introduction

Deep Neural Networks (DNNs) have achieved great success in various applications, such as image classification, object detection, segmentation, etc. Due to the rapid growth of edge intelligent applications, there has been a growing interest in deploying DNNs to edge devices, especially for applications with real-time constraints and privacy issues. With the rapid growth of model parameters, the on-chip cache of existing accelerators often cannot store all model parameters

and activations [26, 28]. Consequently, the accelerators need to access off-chip DRAM frequently, resulting in increased latency and power consumption.

To achieve low-power computing, it is generally necessary to begin with model optimization and develop hardware-friendly compression algorithms. However, existing model compression methods face challenges in balancing compression rates and accuracy. For instance, 1-bit quantization reduces the model size by 32 \times , but low-bit quantization can cause significant quantization errors, leading to a significant drop in accuracy. Unstructured pruning [10, 22, 27] has to store the indices of unpruned weights while the pruning rate of structured pruning [18, 25] rarely exceeds 50%. Vector Quantization (VQ), by grouping and clustering weights, has the potential to achieve higher compression ratios and is a hardware-friendly compression method. However, existing vector quantization works [2, 9, 23, 31, 33, 36] treat all weights equally. As a result, many important weights are forced to align with unimportant weights, leading to numerous clustering errors and significant accuracy degradation.

To achieve extreme compression of neural network models while keeping high accuracy and hardware-friendliness, a Masked Vector Quantization (MVQ) method is proposed. Our method aims to better approximate the important weights in DNNs. The first step in the codebook generation process is the N:M pruning, where unimportant weights are removed. The masked k-means algorithm is then applied to prevent unimportant weights from interfering with the vector clustering process. Only unpruned weights in subvectors need to be computed with codewords. The codewords are then updated. Quantization is applied to the codebook to ensure hardware-friendliness. Codewords of the codebook can be fine-tuned by masked gradients from corresponding subvectors of compressed weights.

To fully leverage the potential of our MVQ compression method, we propose a SW-HW co-designed accelerator based on the EWS dataflow [35]. This architecture incorporates an assignment-aware weight-loading controller to minimize the DRAM data access cost, along with a sparsity-aware systolic array that significantly reduces computing resources. This architecture facilitates achieving high area and energy efficiency.

Experimental results indicate that when our MVQ algorithm is applied to various models, it not only improves accuracy but also reduces FLOPs compared to conventional VQ methods. Our accelerator is synthesized using a 40 nm 0.99V library. In comparison to the base EWS accelerator, our MVQ accelerator enhances energy efficiency by 2.3 \times and reduces the size of the systolic array by 55%. Furthermore, our accelerator outperforms previous sparse accelerators, achieving over 1.73 \times higher efficiency.

The main contributions of the paper are summarized as follows:

- We introduce a novel compression pipeline and the masked vector quantization algorithm to better approximate important weights during vector clustering.
- We propose an area- and energy-efficient hardware accelerator for this MVQ compression algorithm.
- We validate the accuracy improvement of our algorithm as well as the efficiency gains of our accelerator.

2 Related Work

In this section, we first provide a brief review of popular compression techniques for convolutional neural networks. Then, we review related ASIC accelerators and Hardware-Software (HW-SW) co-design approaches for efficient inference.

2.1 N:M Pruning.

The fine-grained N:M pruning technique performs unstructured pruning within each group while enforcing an additional constraint that only N values are pruned. N:M sparsity can be accelerated on modern hardware (Nvidia Ampere Sparse Tensor Core [24]) while maintaining high sparsity. [38] trains the N:M sparse model with uniform sparsity from scratch. [34] finds mixed layerwise N:M sparsity patterns to achieve higher accuracy and compression ratio.

2.2 Vector quantization.

Instead of storing weights themselves, vector quantization stores a codebook and a list of assignments. The compressed weight is reconstructed by looking up the codeword in the codebook that corresponds with the assignment. BGD [33] uses the product quantization [13] method and adopts activation into clustering to minimize reconstruction error. Additionally, layer-wise fine-tuning of codewords via distillation is applied to ensure that the output of each layer is similar to that of the pre-trained model. PQF [23] focuses on identifying parameter groups to compress together, searching for optimal permutations to enable efficient compression. DKM [4] casts k-means clustering as an attention problem and enables joint optimization of the DNN parameters and clustering centroids. However, in conventional vector quantization, a problem arises when important and unimportant weights align within subvectors, causing significant errors and decreased accuracy.

2.3 Systolic Array-based accelerators for CNNs

Designing dedicated dataflows to fully utilize the data reusability in CNN for memory access optimization is a significant research topic in using systolic array-based CNN accelerators. TPU [14] is a WS dataflow accelerator proposed by Google. It parallelly unfolds in the input channel(C) and output channel(K) of the convolution kernel, also known as the C|K unfolding. Gemmini [7] further reduces the number of pipeline registers and pipeline latency in the systolic array by introducing adjacent PE to form a combinational logic

addition tree of tiles. EWS [35] observes the problem of frequent array accesses to global buffers caused by insufficient data reusability in WS data flow CNN accelerators with C|K unfolding. It proposes an Enhanced Weight Stationary (EWS) that fuses IS and OS strategies.

2.4 Accelerators with compression-based co-design

Another hot topic is HW-SW co-design accelerators based on various model compression techniques. [20] proposed a Systolic Tensor Array (STA), based on the N:M pruning, operating with OS data flow. When using 2:4 pruning, only 2 multipliers and 1 adder are needed to implement 4×4 vector dot product operations, reducing the computational resources by about half compared to non-sparse models. [21] further exploit Density Bound Block (DBB) sparsity for both weights and activations. [12] explores efficient signed bit-slice architecture with signed bit-slice representation (SBR) for efficient dense DNN acceleration. [17, 37] design vector quantization-based accelerators, but their vector quantization algorithms suffer significant accuracy degradation, and the implemented accelerators do not optimize the dataflow specifically based on the parameter characteristics of CNNs.

3 Preliminaries

For a typical vector quantization algorithm, $B \in R^{NG \times d}$ denotes a 2D data matrix, $C = \{c_1, \dots, c_k\}$ denotes the codebook containing k codewords of size d . We can view B as a collection of NG subvectors of dimension d . Each subvector $b_j \in B$ is mapped to one of the codewords $c_i \in C$, the function can be represented as $q(b_j) = c_i$. In the subsequent sections of this article, we will consistently represent the number of codewords as k , the block size (length of a codeword) as d , and the number of subvectors as NG .

To minimize the Sum of Square errors (SSE), the most popular approach is the k-means clustering algorithm. The basic procedure of k-means is as below:

1. Randomly select k subvectors as initial codewords.
2. For each subvector, calculate the Euclidean distance between itself and every codeword, then assign itself to the nearest codeword.
3. For each codeword, calculate the average value of subvectors assigned to it.
4. Repeat step2 and step3 until the number of changing assignments falls below a given threshold, which is typically set to 0.1% of the total number of subvectors.

4 Masked Vector Quantization

In this section, we first conduct empirical experiments to reveal reducing clustering errors of important weights is crucial to model performance. Then, we present our masked vector quantization pipeline in detail.

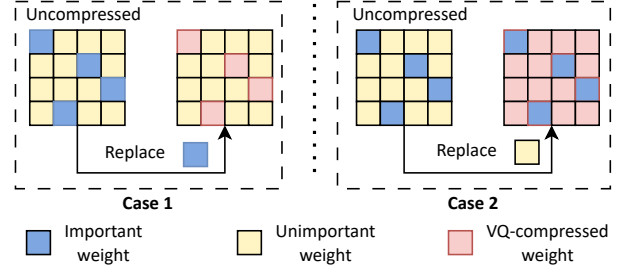


Figure 1. Two cases to replace some weights with corresponding vector-quantized ones

Methods	ResNet-18		ResNet-50	
	SSE	Acc	SSE	Acc
Case 1	576	5.8	695	1.26
Case 2	623	37.46	771	55.39

Table 1. Partly vector-quantized accuracy on ImageNet dataset across two cases and different models. Note that we didn't perform any fine-tuning in this experiment.

4.1 Empirical observation

To investigate the influence of clustering errors on different weights, we conduct preliminary experiments on the ImageNet dataset. We present a simple visualization in Fig. 1 illustrating two scenarios of introducing clustering errors to weights of varying significance. We select 2 weights with the highest magnitude within each of the 8 continuous elements. These selected weights, which account for 25% of total weights, are marked as important weights, while the others are marked as unimportant weights. We perform a layerwise vector quantization for convolutional layers with $k = 512$ and $d = 8$ and obtain vector-quantized weights. We replace part of the weights with their corresponding quantized weights. In Case 1, important weights are replaced with their vector-quantized weights, while in Case 2, the remaining unimportant weights are replaced with their vector-quantized weights. Without any fine-tuning, we evaluate the top-1 accuracy and SSE and summarize the results in Tab. 1. Even though case 2 exhibits higher SSE, it achieves significantly higher accuracy than that of case 1. Therefore, we can conclude that approximating important weights during vector quantization plays a dominant role in the preservation of model performance. Simply reducing overall clustering error leads to a suboptimal solution.

4.2 Overview of MVQ

Based on the conclusion from the previous subsection, our method prioritizes minimizing errors for important weights. To accomplish this, we propose MVQ, which uses pruning to remove unimportant weights. Then, pruning masks are used in the masked k-means process to avoid aligning important

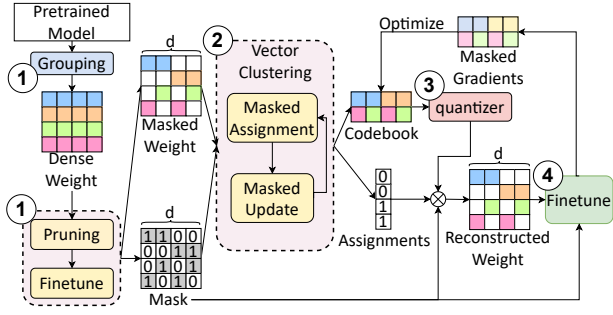


Figure 2. Overall compression pipeline of our MVQ algorithm. 1. The grouping strategy is determined for both pruning and vector clustering. Pruning is performed and the sparse model is fine-tuned. 2. Unpruned weights and the mask are incorporated into the masked k-means algorithm to generate the codebook. 3. Symmetric 8-bit quantization is applied to the codebook to ensure hardware-friendliness. 4. The codebook is fine-tuned with masked gradients.

weights with unimportant ones. As illustrated in Fig. 2, our compression pipeline consists of four steps:

1. **Weight grouping and pruning:** The codebook’s encoding is established and weights are divided into groups. Subsequently, less important weights are removed through pruning.

2. **Masked k-means clustering:** To avoid the influence of these pruned weights, the masked k-means algorithm is applied to execute vector clustering.

3. **Codebook quantization:** Symmetric 8-bit quantization is applied to the codebook to ensure hardware-friendliness.

4. **Finetuning:** To recover the accuracy of the compressed model, codewords are fine-tuned using masked gradients.

Detailed explanations of these steps will be provided in the following subsections.

4.3 Weight grouping and Pruning

To perform subsequent vector clustering, weight W has to be firstly grouped to a set of subvectors with length d . As illustrated in Fig. 3, the 4D weight can be split and grouped into a set of vectors in different dimensions, including kernel dimensions, input-channel dimensions, and output-channel dimensions. The group length d is constrained to $k * k$ for kernel dimensions, however, the group length of both output-channel-wise and input-channel-wise grouping is more flexible, i.e., it could be a power of 2. In pursuit of a higher compression ratio and hardware efficiency, the channel-wise grouping strategy is chosen. In this way, the 4D weight is reshaped into a 2D matrix W_r of size $(\frac{C_{out}}{d} \times C_{in} \times k \times k) \times d$.

After grouping, N:M pruning, which achieves a high level of sparsity while maintaining a regular sparse structure, is applied. For each subvector in W_r of length d , $\frac{(M-N) \times d}{M}$ elements are pruned, and d must be multiples of M . The sparse

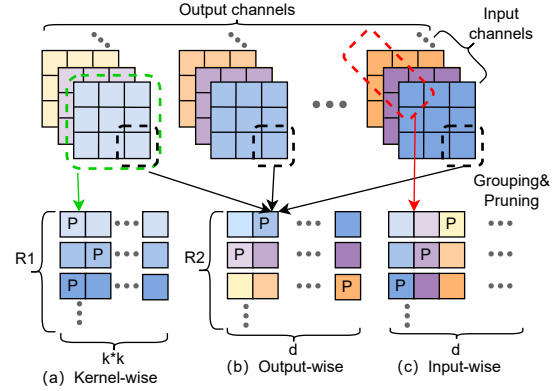


Figure 3. An illustration of grouping strategies. For kernel-wise grouping, $R_1 = C_{out} \times C_{in}$. For input and output-channel-wise grouping, C_{out} and C_{in} are multiples of d , and $R_2 = \frac{C_{out}}{d} \times C_{in} \times k \times k$.

model is then fine-tuned before undergoing the vector clustering process. Additionally, a bitmask denoted as BM is saved to indicate the positions of the pruned and unpruned weights. The same grouping strategy applied to weights reshapes M to M_r . The 2D weight matrix after pruning and fine-tuning is denoted as W_{rp} . Each subvector w_j from W_{rp} is assigned to one of the codewords, namely $q(w_j) = c_i$, where i is the assignment. The corresponding mask of w_j is denoted as bm_j . The detailed settings of pruning strategies and fine-tuning strategies will be discussed in Section 6.2.

4.4 Masked k-means clustering

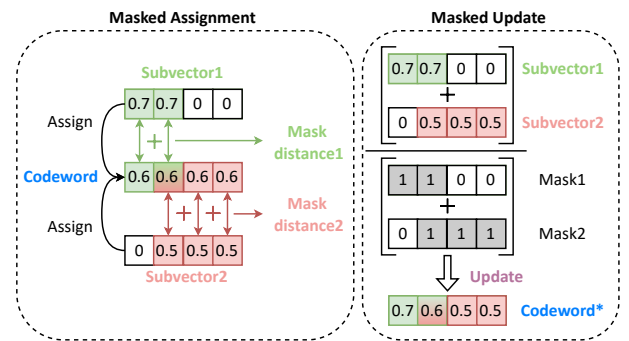


Figure 4. A simple example of masked k-means. For subvector1 and subvector2 assigned to the same codeword, green blocks represent unpruned weights in subvector1, while red blocks represent unpruned weights in subvector2. During the masked assignment step, only the unpruned weights in subvectors are used to calculate distances with the codeword. During the masked update step, only unpruned weights are involved in updating the codeword.

Upon obtaining the sparse model and its corresponding mask, our objective is to minimize the clustering error for

important weights by minimizing the following objective function:

$$\|W_{rp} - \widehat{W}_{rp}\|_2^2 = \sum_j \|w_j - q(w_j) \circ bm_j\|_2^2 \quad (1)$$

Therefore, the codebook and assignments can be learned using the k-means algorithm. However, if common k-means clustering (as discussed in preliminaries) is applied to W_{rp} , many important weights have to be aligned to zero, making it difficult to reduce the clustering error for these weights (this phenomenon will be further demonstrated in the ablation study section). To reduce the impact of pruned weights, our masked k-means algorithm replaces these two steps with the masked assignment and the masked update:

Masked assignment. Each subvector w_j is assigned to the nearest codeword c_i such that

$$c_i = \arg \min_{c \in C} \|w_j - c \circ bm_j\|_2^2 \quad (2)$$

As shown in Fig. 4, only the unpruned weights in w_j are considered when calculating the Euclidean distance from weight subvector to each codeword. This step can be computationally intensive as the codebook needs to be multiplied with different masks for each subvector. To efficiently implement this step on GPU, we use the broadcasting mechanism in PyTorch. we construct a tensor of shape $[L, k, d]$ to depict the application of different masks on each codeword. Then, we employ *torch.cdist* function to compute its Euclidean distance with the weight matrix. Additionally, we use batch processing to reduce memory consumption.

Masked update. Let v_p denote the subvectors that are currently assigned to c_i . Let n_p denote the mask for v_p . The update of the codeword is a least square problem, and its analytical solution is the average of corresponding subvectors.

$$c_i^* = \arg \min_{c_i \in R^d} \sum_p \|(v_p - c_i) \circ n_p\|_2^2 \quad (3)$$

The pruned weights don't rely on the codeword for reconstruction because they are permanently zero. Therefore, in the masked update step, the condition in the least squares problem is changed to Eq. 3. The analytical solution to Eq. 3 is computed as follows:

$$c_i^* = \frac{\sum_p v_p}{\sum_p n_p} \quad (4)$$

As shown in Fig. 4, different from simply averaging v_p , only the average of the unpruned element is calculated, which prevents the great amount of 0 values from disturbing c_i^* . Division in Eq. 4 refers to element-wise division. Once the vector clustering is done, the assignments and the bitmask are fixed. Detailed vector clustering error comparison will be provided in the ablation study section.

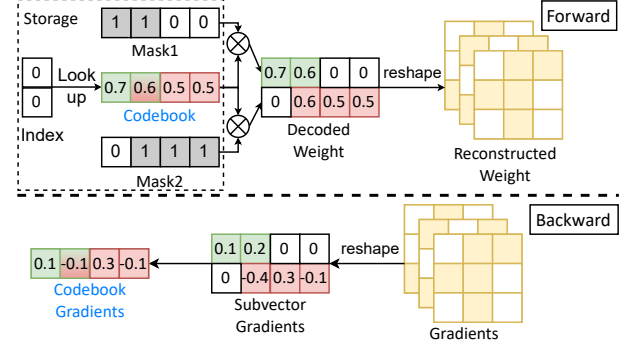


Figure 5. A simple example of the fine-tuning process. Weights are reconstructed from the codebook, assignments, and masks for forward computation, while masked gradients are calculated to update the codebook.

4.5 Codebook quantization

Quantization can be further applied to the codebook. Given the full-precision data v , the scaling factor s , and the quantization bits qb , the symmetric uniform quantized representation \hat{v} is calculated as :

$$\hat{v} = s_w \times \text{clamp}\left(\left\lfloor \frac{v}{s_w} \right\rfloor; -2^{qb-1}, 2^{qb-1} - 1\right) \quad (5)$$

To ensure hardware compatibility, signed 8-bit quantization as illustrated in Eq. 5 is applied. One codebook share the same s_w , and LSQ [5] is used to determine s_w . For large values of k , the storage cost of the codebook itself becomes an unignorable factor. Quantizing the codebook also helps to reduce this cost.

4.6 Fine-tuning method

To restore the network's original accuracy, it is crucial to fine-tune the codebook. Our method's final storage comprises three components: assignments, codebooks, and masks. During the forward pass, as depicted in Fig. 5, codewords retrieved from the codebook perform a bit selection operation with their corresponding mask to obtain decoded weights. These decoded weights can be reshaped back to 4D reconstructed weights, which are then used in forward computation.

During the backward propagation, let $Loss$ be the loss function of the network. Note that $Loss$ is differentiable to each of the learned centroids. As shown in Fig. 5, to avoid the distribution of zero gradients of pruned weights, masked gradients are computed for each codeword, in a similar form to Eq. 4. Then, gradients-based learning is performed as follows :

$$c_i \leftarrow c_i - O\left(\frac{\sum_p \frac{\delta Loss}{\delta v_p} \circ n_p}{\sum_p n_p}, \theta\right) \quad (6)$$

where $O(\cdot)$ is the optimizer (Adam [15], SGD, AdamW) with hyperparameter θ (learning rate, momentum, weight decay).

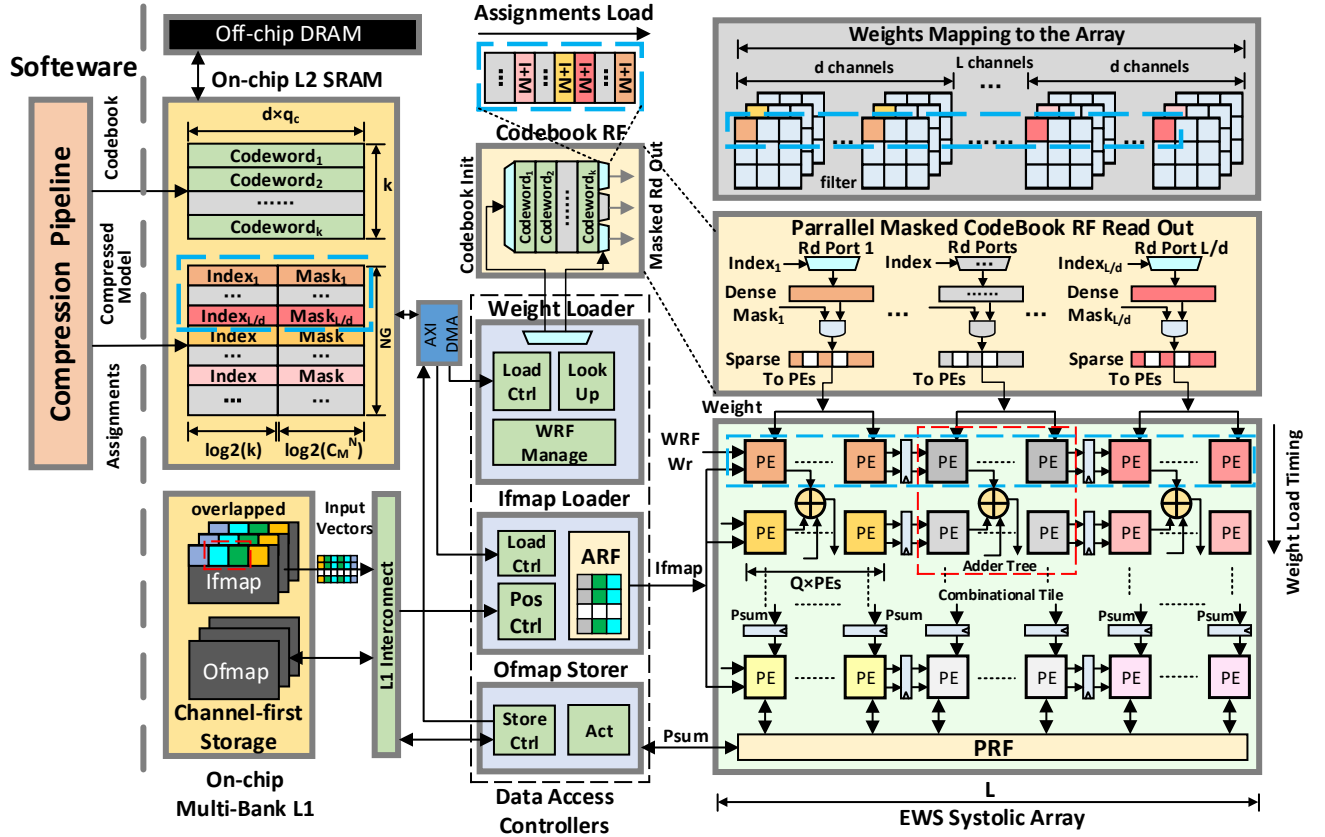


Figure 6. Overview of our efficient accelerator with masked vector quantization.

5 Accelerator Implementation for MVQ

In this section, we display our hardware microarchitecture design and showcase the hardware-software co-design involving masked vector quantization. Denote b_f as the bit-width of full-precision weight. Given a weight block and a mask block of the same size $NG \times d$. The Compression Ratio of our method is calculated as:

$$Comp.Ratio = \frac{NG * d * b_f}{b_a + b_m + b_c} \quad (7)$$

where b_a , b_m , and b_c are the storage costs of assignments, masks, and codebooks, respectively. Assuming that the weight block is clustered into k codewords and the codebook is quantized to q_c bits, we can calculate $b_a = \lceil \log_2(k) \rceil \times NG$ and $b_c = k \times d \times q_c$. Note that b_c is relatively small, quantizing the codebook noticeably improves the compression ratio only when k is very large. As for b_m , storing the complete bitmask requires one bit per weight, which is unbearable for extreme compression. Since a N:M pruned block contains only C_M^N combinations of masks, a look-up table could be created, reducing the storage cost to $\frac{\lceil \log_2 C_M^N \rceil}{M}$ bit per weight.

5.1 Architecture Overview

After obtaining the compressed model through the method in Section 4, we load the two parts of the model: Codebook and Assignments (including the index and mask required to reconstruct each weight vector of length d) from the off-chip memory to the on-chip L2 SRAM. An overview of our accelerator is shown in Fig. 6. The accelerator consists of data access controllers (Weight/Ifmap Loader and Ofmap Storer) that support EWS dataflow, a systolic array with combinational tile referring to Gemini [7] and PE with Weight Register Files (WRF). The data access controllers implement data interaction between L2 and L1 and the array through DMA with a datawidth of 64-bit. L1 is a global buffer composed of multiple SRAM banks, providing the accelerator with enough datawidth to read Ifmap and store Ofmap/Psum with a single-cycle delay.

The EWS dataflow deployed by the accelerator refers to the implementation in [35], as described in Fig. 7. Given the parameters of a convolution layer, compared with the conventional WS, EWS introduces a three-dimensional layer-wise optimizable extension in the red box, which can further split the three dimensions of output channel, input channel and kernel plane by integrating them into the inner loop of

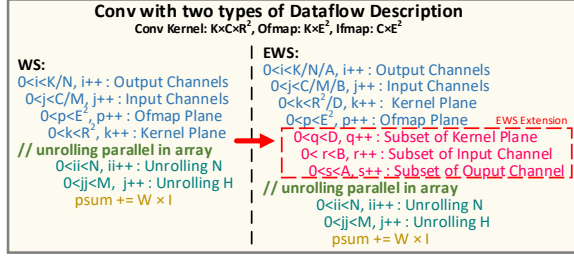


Figure 7. Brief description of EWS dataflow

feature map plane traversal: In every consecutive A cycles, the activations fetched by systolic array stays in the PEs, so that the PEs can switch weights from the WRFs inside them to multiply with the same activations and get psums corresponding to $N \times A$ output channels. Then in every consecutive $A \times B$ cycles, weights corresponding to B input channels are switched, the accumulated psums can be read or written in the PRFs instead of on-chip SRAM. Finally, D coordinates on the convolutional kernel plane is traversed in consecutive $A \times B \times D$ cycles. As a result, during the traversal of this subset with $A \times B \times D$ weights, the frequency of accessing activation and partial sum from on-chip SRAM can be reduced to the original $1/(A \times D)$ and $1/(B \times D)$ respectively. The extensions A and B can make the PE array with the physical size of $H \times L$ have data reuse the same as that of $(H \times B) \times (L \times A)$ array. The extension D supports the WRF in storing multi-element convolution kernel plane subsets. The Activation Register File (ARF) and Partial Sum Register File (PRF) in Fig. 6 provide architectural support for the convolutional reuse of Ifmap and channel-wise partial sum accumulation, respectively. To handle the potential splitting and merging of feature maps in the channel, width, and height dimensions during convolution calculation, a specialized DMA is employed, capable of directly transferring 3D tensors between L2 and L1. The controller and load/store components can initiate transfer requests to the DMA through the DMA interconnect, which can respectively handle state queries and data access instructions.

5.2 Assignment-aware Weight Loading

To harvest gains for efficient inference from the MVQ compressed model, we have developed a set of methods to map the compression model to the accelerator.

Before the inference starts, the Weight Loader initializes the codebook to the Codebook Register File (CRF) through DMA. Considering that the size of the codebook is usually only at the KB level, and the codebook only needs to be updated once when a layer or even the entire network is executed, the delay and energy overhead caused by initializing the CRF is negligible. The MVQ model requires the assignment of reconstructing a weight vector with a dimension of d . Therefore, we integrate the reconstruction of weight

vectors into the loading assignment process. Weight Loader reads assignments from L2. The index is used as the address to read CRF, and the mask is stored in $\log_2(C_M^N)$ bits. After restoration through the Look Up Table (LUT) in the Weight Loader, the sparse mask with d bits is obtained. The sparse reconstructed weight is obtained through the AND gates.

Considering that the width L of the systolic array (corresponding to the parallelism on the convolution output channel) may not be the same as the length d of the weight vector in the MVQ method, a row of PEs requires L/d weight vectors, so the CRF is designed with L/d read ports. In addition, the storage format of the assignments stored in L2 is aligned with the hardware array width L , as shown in the blue box in Fig 6: Each color block represents a d -dimensional weight vector corresponding to d output channels.

5.3 Sparsity-aware Systolic Array Design

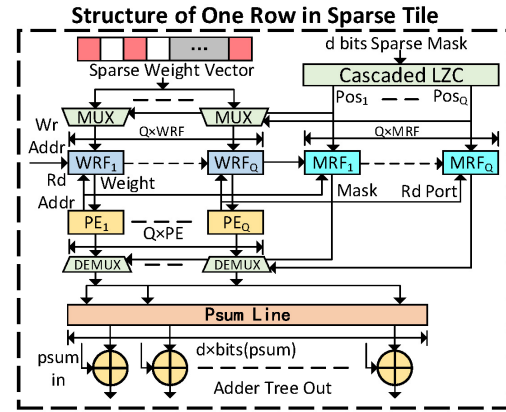


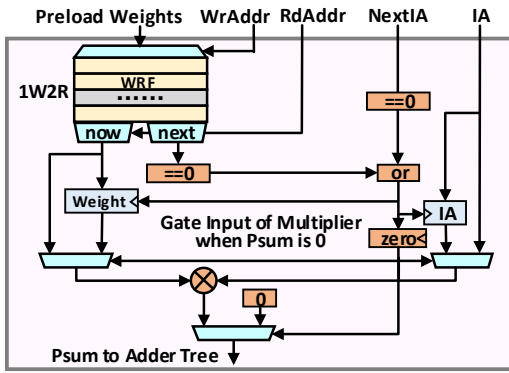
Figure 8. Implementation of the sparse tile.

Every weight subvector written into the systolic array employs $N:M$ sparsity, however, the computation of 0 elements is meaningless. For EWS dataflow, since the weights in the systolic array are stationary, only $Q = \frac{N}{M} \times d$ numbers of PEs are running in a PE group corresponding to a subvector. Theoretically, we only require $\frac{N}{M}$ of the original computing sources, which means Q PEs for every d output channel.

Every $N:M$ sparsity mask contains N valid bits and thus can't be encoded with a common one-hot encoder. We employ Q numbers of LZC (Leading Zero Counter) to encode the sparsity mask with Q valid bits. Each output encoding of LZC is converted into one-hot encoding and sent to the next level LZC with the XOR logic of the input mask at the current level. Q LZCs are cascaded to form the encoder of the sparsity mask.

The implementation of the sparse tile is illustrated in Fig. 8. For a simple explanation, we separate the registers in the PE to the outside of the PE. Based on Q PEs and Q Weight Register Files (WRFs), Q Mask Register Files (MRFs) with a storage bit width of $\log_2 d$ are introduced. The cascaded

Methods	EWS	EWS-Sparse
Multiplier	$H \times d$	$H \times Q$
Adder	$H \times d$	$H \times d$
RF	$H \times d \times 16 \times b_w$	$H \times Q \times 16 \times b_w + H \times Q \times 16 \times \log_2 d$
LZC	NA	$H \times Q$
DEMUX	NA	$H \times Q \times b_{psum}$
MUX	NA	$H \times Q \times b_w$
Parallelism	$2 \times H \times d$	$2 \times H \times d$

Table 2. Resources Comparison for a $H \times d$ Tile

Figure 9. Implementation of the PE with zero value gating.

LZC encoder receives d -bit sparsity masks dispatched to the tile by the weight loading controller as input, and Q position encodings are output and written to the MRF. The MRF and WRF are written and read simultaneously, which simplifies the implementation of the control logic: MRF and WRF share the write address and write enable signals from the array controller, and also share the read address signals from the PE. The output of the multiplier in the PE needs to be coordinated with Q DEMUXs and the MRF output sparsity position encoding that shares the read address with the WRF. These Q partial sums are then distributed to the corresponding partial sum positions as the input for adder trees with a depth of d .

The resources cost of an $H \times d$ tile is summarized in Tab. 2. Compared with EWS, our EWS-Sparse greatly reduces the cost of multiplier and register files while maintaining the same computability with sparse models.

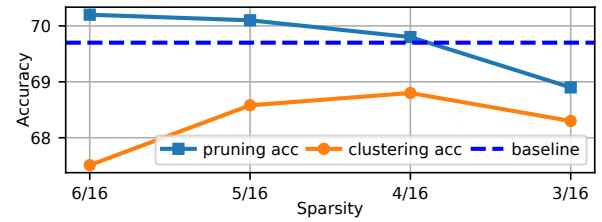
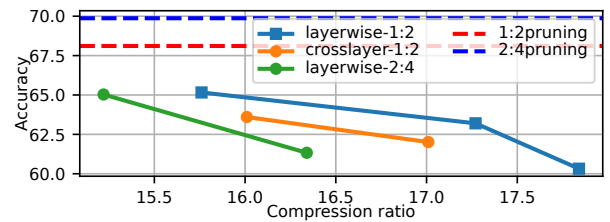
To further reduce energy consumption, a zero-value gated PE is implemented to reduce the flip rate of MAC. Quantized weights and input activations naturally exhibit sparsity, if either one is zero in the same computation cycle, the partial sum for this computation will also be zero. The implementation is illustrated in Fig. 9. The WRF of the PE is designed with two sets of read ports: one for reading the weights required for the current computation, and another for prefetching the

next weight value. This prefetching allows for the determination of whether the subsequent weight value is zero. A similar approach is applied to the input features. When the partial sum of the next cycle is zero, the weight and input stored in registers will be selected, and the input value of the multiplexer at the next cycle will remain unaltered. Consequently, the switching power consumption of multiplexers can be reduced.

6 Performance Analysis for masked vector quantization Algorithm

6.1 Experiment setup

In our experiments, the accuracy and storage cost are evaluated as key metrics. We commence our experiments by discussing the appropriate pruning strategy. We then perform a detailed ablation study to assess the effect of our masked vector quantization method. Once the optimal compression settings are obtained, we compare the accuracy and FLOPs between our method and other advanced compression techniques on a large set of models.


Figure 10. Pruning strategy experiments on ResNet-18.

Figure 11. Pruning strategy experiments on MobileNet-v2.

6.2 Pruning strategy

When the pruning rate is higher, the accuracy of pruning decreases, while the clustering error becomes smaller, narrowing the gap between clustering accuracy and pruning accuracy. Also, different pruning patterns affect the storage cost of masks. Therefore, in our work, selecting a pruning strategy is complex and involves multiple trade-offs. For classification tasks, we train the sparse model using SR-STE, following the training settings in [34]. For detection and segmentation tasks, we found that SR-STE is unstable and less effective. Therefore, we simply used the ASP method.

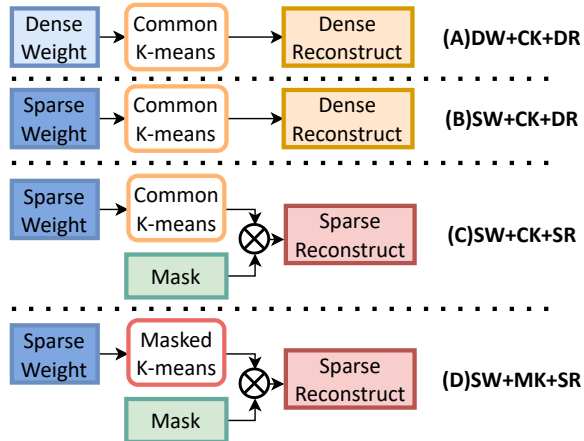


Figure 12. Illustration of the four comparing methods in ablation study. ‘DW’/‘SW’ denotes Dense weight/Sparse weight to be vector clustered. ‘CK’/‘MK’ denotes common k-means/masked k-means. ‘DR’/‘SR’ denotes Dense reconstructed weight/Sparse reconstructed weight.

For models with high redundancy (e.g. ResNets), we seek to achieve highest possible pruning rate while maintaining accuracy, as a higher pruning rate leads to smaller clustering errors. As illustrated in Fig. 10, pruning rates spanning from 6:16 to 3:16 were tested on ResNet-18. The pruning accuracy rapidly drops below the baseline after sparsity exceeds 75%. Ultimately, 4:16 pruning yields best clustering accuracy.

For parameter-efficient models (e.g. MobileNets and EfficientNets), 50% sparsity already results in a notable decline in pruning accuracy. We conducted experiments on MobileNet-v2, exploring both 1:2 and 2:4 pruning. The 2:4 pruning approach demonstrated a 1.7% higher pruning accuracy but came with 0.25bit/w additional mask storage cost compared to 1:2 pruning. Our findings suggest that 1:2 pruning may offer a more optimal balance between storage and accuracy.

6.3 Ablation study

A comprehensive ablation study is conducted on ResNet-18 to analyze and evaluate the impact of pruning on the vector clustering process. We compare four cases, which are shown in Fig. 12. Case (A) represents the simplest vector quantization procedure. For the first two cases, (A) and (B), the mask is not involved in reconstructing compressed weights, so it doesn’t need to be stored and there is no reduction in FLOPs. The difference between them is that sparse weights are clustered in (B). Storing the mask is required for cases (C) and (D) to reconstruct sparse weights and reduce FLOPs. Our method, represented by (D), uses masked k-means for vector clustering, which distinguishes it from the other three methods.

To reconstruct sparse weights, the bitmask needs to be stored. To ensure a fair comparison in terms of compression

Cases	Total/Mask SSE	Flops	Acc (FP:69.7)
A	1153/463	1.81G	66.5
B	518/498	1.81G	67.3
C	1840/1840	0.54G	61.1
Ours	251/251	0.54G(-70%)	68.8 (+1.5)

Table 3. Ablation study on ResNet-18: We ensure the same compression ratio of $\sim 22x$ for 4 cases.

Models	CR	Methods	Acc	Sparsity	FLOPs
SSL-		MVQ(Ours)	77.5	75%	1.11G
ResNet-50	$\sim 22\times$	PQF [23]	77.1	0%	4.09G
Acc: 79.2		BGD [33]	76.1	0%	4.09G
MobileNetV1	$\sim 17\times$	MVQ(Ours)	66.3	50%	0.29G
Acc: 70.8	$\sim 19\times$		64.3	50%	0.56G
MobileNetV2	$\sim 16\times$	MVQ(Ours)	65.1	50%	0.15G
Acc: 71.7		PvQ [16]	59.1	0%	0.30G
EfficientNet	$\sim 16\times$	MVQ(Ours)	68.2	50%	0.14G
Acc: 75.4		PvQ [16]	60.9	0%	0.28G
AlexNet	$\sim 25\times$	MVQ(Ours)	55.4	75%	0.19G
Acc: 56.5					
VGG-16	$\sim 28\times$	MVQ(Ours)	69.7	81%	2.90G
Acc: 71.7	$\sim 34\times$		68.8	88%	1.96G

Table 4. Comparison with other methods on more models. ‘CR’ denotes Compression Ratio.

ratio, we set $k = 1024$ (Resp. $k = 512$) and $d = 8$ (Resp. $d = 16$) for Case A&B (Resp. C&D). We use Total SSE to indicate the cluster error of all weights and Mask SSE to indicate the cluster error of masked weights. When comparing the results of (A) and (B) in Tab.3, it is observed that applying sparse weights significantly reduces the total clustering error, but the clustering error for important weights remains large. This indicates that important weights are still forced to be aligned to many zeros. Our proposed method (D), which combines pruning and masked k-means, reduces the clustering error by 85% compared to case (C). This suggests that the codewords can better approximate the important weights by using masked k-means.

Next, the accuracy and FLOPs of the four methods are evaluated. The results are tabulated in Tab. 3. The results of case (C) show that the conventional k-means clustering method is ineffective in reconstructing sparse weights with a restricted number of centroids. Our method improves accuracy and reduces FLOPs compared to (A) and (B), even with fewer codewords. This indicates that the cost of storing masks is worthwhile.

6.4 Comparison with other methods

In this subsection, We compare exclusively on ResNets and MaskRCNN with previous VQ-based methods, including BGD [33], PQF [23]. For other models not compressed by PQF, we compare with PvQ [16] which conducts uniform scalar quantization on a larger set of models.

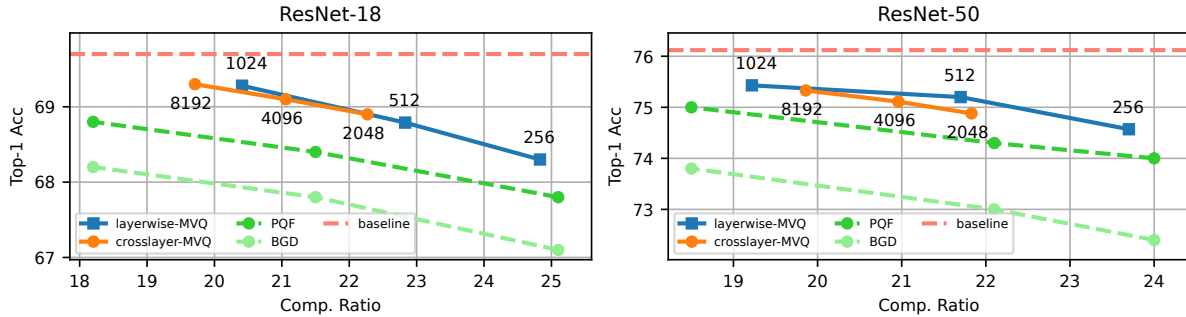


Figure 13. Comparison with previous VQ-based methods on ResNet-18 and ResNet-50.

Methods	ResNet-18		ResNet-50	
	SSE	Acc	SSE	Acc
PQF [23]	605	68.2	1150	74.2
Ours	251	68.8	336	75.2

Table 5. Comparison of the SSE and accuracy between our method and previous vector quantization approach at $\sim 22\times$ compression ratio. SSE is evaluated before fine-tuning.

Image Classification. Accuracy and compression ratio results on ImageNet are presented in Fig. 13 and Tab. 4. We conduct experiments on both layerwise clustering (i.e. using one codebook for each layer) and crosslayer clustering (i.e. employing one codebook for all convolutional layers). Our results indicate that layerwise clustering yields a superior memory-accuracy trade-off. Our method outperforms all counterparts on a diverse set of models. For example, on the ResNet-18, our method delivers an accuracy improvement of 0.5% to 0.8% over PQF at compression ratios between $20\times$ and $25\times$. Similarly, for the ResNet-50, our method reaches 75.2% accuracy at a $\sim 22\times$ compression ratio. This represents a 1.0% improvement over the state-of-the-art. Furthermore, On MobileNets and EfficientNet, our approach demonstrates superior results compared to 2-bit uniform quantization. In addition to the increase in accuracy, our method also significantly reduces FLOPs by about 70% (50% for parameter-efficient models).

To clarify how our method achieves greater accuracy than other weight clustering methods with the same compression ratio, we conduct a comparison of SSE between our work and PQF. The results are shown in Tab. 5. At the same compression ratio, our method reaches a significantly lower SSE than PQF, especially on ResNet-50, which results in smaller accuracy degradation.

Object Detection and Segmentation. Our method is also validated on the task of object detection and segmentation. We compress the ResNet-50 Mask-RCNN FPN architecture using the MS COCO 2017 dataset [19]. The results are represented in Tab. 6. Our method achieves a box AP of

MaskRCNN on COCO2017 dataset					
Methods	CR	Sparsity	FLOPs	AP^{bb}	AP^{mk}
Baseline	-	0%	88.9G	37.9	34.6
BGD [33]	$26\times$	0%	88.9G	33.9	30.8
PQF [23]	$26\times$	0%	88.9G	36.3	33.5
Ours	$26\times$	75%	23.4G	36.8	33.8

DeepLab-V3 on VOC dataset				
Methods	CR	Sparsity	FLOPs	mIoU
Baseline	-	0%	4.2G	72.9
PvQ [16]	$16\times$	0%	4.2G	17.6
Ours	$19\times$	50%	2.1G	66.5

Table 6. Comparing bounding box and mask metrics on COCO 2017 with other vector quantization methods. FLOPs are calculated with an input size of [3,800,800] for COCO and [3,512,512] for VOC

36.8, and a mask AP of 33.8 at $26\times$ compression ratio. Additionally, our method reduces the FLOPs by 70% compared with previous vector quantization methods. We also compress DeepLab-v3 [1] with MobileNet-V2 backbone trained for semantic segmentation on Pascal VOC [6]. Our MVQ maintains a high mIoU at $19\times$ compression ratio while 2bit uniform quantization crashes.

7 Hardware Implementation Experiments and Performance Evaluation

7.1 System setup

We consider the open-source PULP [26] framework to validate the performance of our accelerator. Our system consists of a main control System-on-Chip (SoC) and an accelerator subsystem built around a customized systolic array used for DNN inference acceleration. The detailed mechanism of SoC and hierarchy caches has been discussed in [35]

To assess the inference performance of our accelerator, we conducted tests by running five CNN models (ResNet-18, ResNet-50, VGG-16, AlexNet, MobileNet-v1) on three scales of PE arrays (16×16 , 32×32 , and 64×64). Throughout, we compare designs in terms of area efficiency, speedup, and energy efficiency. Our ASIC design was synthesized using the

		Size-16	Size-32	Size-64
Accelerator	WS	0.188	0.734	2.812
	EWS	0.36	1.14	4.236
	EWS-C/CM	0.650	1.505	4.776
	EWS-CMS	0.469	0.828	2.129
L1		0.484	0.968	0.968
L2		6.924		
Others		0.787	1.303	1.659

Table 7. Area comparison on 3 array scales

Synopsys Design Compiler with a 40 nm 0.99V LVT Library. The accelerator’s performance was assessed through gate-level netlist simulation, while power consumption during operation was evaluated using Synopsys Prime Time PX (PT).

For a thorough comparison, we conducted tests using 6 different hardware settings based on WS and EWS dataflow:

(a) WS(WS-base): This is the baseline setting for WS dataflow where weights are simply quantized to 8-bit.

(b) WS-CMS: This setting fully utilizes MVQ within WS dataflow.

(c) EWS(EWS-base): This is the baseline setting where weights are simply quantized to 8-bit.

(d) EWS-C: This setting uses common vector quantization [23, 33] to compress weights.

(e) EWS-CM: This setting utilizes our proposed masked vector quantization to compress weights.

(f) EWS-CMS: This setting involves updating sparse tiles based on the EWS-CM approach, i.e., this setting fully utilizes MVQ within EWS dataflow

To ensure a fair comparison in terms of compression ratio, we set $k = 1024$ and $d = 8$ for EWS-C, while $k = 512$ and $d = 16$ for EWS-CM and EWS-CMS.

7.2 Area Analysis

The areas of the accelerator under different hardware settings at 75% sparsity are summarized in Tab. 7, which were obtained through DC synthesis. EWS-C/EWS-CM and EWS-CMS incur an additional area cost for the codebook reg file. As the array size increases, the area of the CRF also increases since it has to support more CRF read ports. However, our EWS-CMS, with its sparse tile implementation, significantly reduces the area cost of the systolic array by 50%-60%. Even with the area cost of CRF, our EWS-CMS for 64×64 array reduces the area by 55% compared to base EWS. Additionally, Tab. 7 includes the area information of L1, L2, and other system components. While L2 is fixed at 2MB, we tested different L1 sizes and found that for 16×16 arrays (Resp. 32×32 and 64×64 arrays), the benefits are limited beyond 128KB (Resp. 256KB). Therefore, we set the L1 size to 128KB for the 16×16 array (Resp. 256KB for the 32×32 and 64×64 arrays). Different areas are observed for other components, including

	DRAM	L2	L1	PRF	ARF	WRF	CRF
Energy	200	15	6	0.22	0.11	0.02	0.02

Table 8. Normalized data access energy cost for different levels of storage. We set the unit cost to a MAC operation.

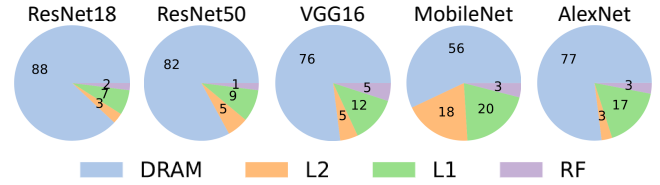


Figure 14. Data access cost ratio of different levels of memory

DMA, peripheral interfaces, and system interconnections, under three array sizes.

7.3 Energy Analysis

Firstly, we model the data access energy cost based on Tab. 8. The DRAM result is obtained from [29] and [3], while the other results are obtained by PT analysis. The data access cost of different levels of memory is presented in Fig. 14, from which it’s clear that DRAM access overhead accounts for the majority. By applying our masked vector quantization technique, the storage cost of 8-bit weights can be greatly reduced, leading to a significant decrease in energy cost for DRAM access. The total data access cost reduction results are

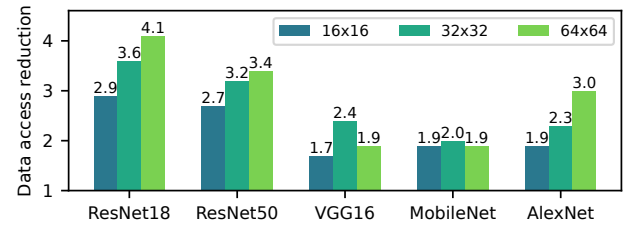


Figure 15. Data access cost reduction by employing MVQ compression

summarized in Fig. 15. By employing MVQ, the access cost of ResNet18 can be reduced up to 4.1×. For MobileNets, our approach also reduces the cost by 2×. We have to mention that for VGG16, input features of the first few layers are too large that they have to be stored in DRAM, thus the reduction ratio is lower than expected.

Secondly, we present a detailed power breakdown of our accelerator. As depicted in Fig. 16. WS has a very high L1 access cost due to insufficient data reusability, which is also why EWS surpasses WS. Benefiting from the sparse tile design, our EWS-CMS/WS-CMS greatly reduces the energy cost of the main accelerator (PE Array), which accounts for the majority of total power consumption. As the array size

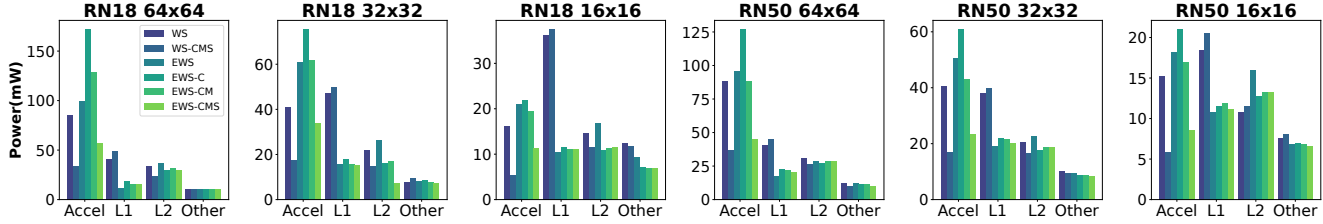


Figure 16. Power consumption breakdown for hardware under test. ‘Accel’ means the main accelerator which consists of the systolic array, controller and RF. ‘Others’ consists CPU, DMA, interface and IO.

increases, the effectiveness of EWS-CMS/WS-CMS becomes more pronounced.

7.4 Performance Analysis

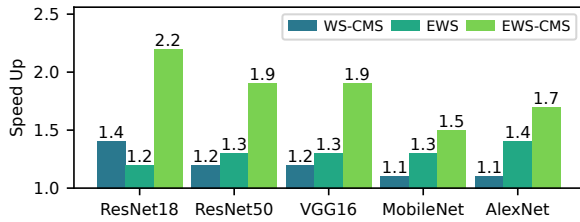


Figure 17. Speed up comparison of different hardware settings on various models. The array size is fixed to 64*64.

Our accelerator also provides a modest speedup. Results are shown in Fig. 17. Our EWS-CMS achieves a 1.2-1.8× speedup over EWS when the array size is set to 64×64. We conducted an analysis using the roofline theory to understand the reason for this improvement. As depicted in Fig. 18, the performance of the accelerator is limited by the weight-loading datawidth for array sizes larger than 32×32. With the aid of our compression algorithm, the datawidth requirement for weight-loading is significantly reduced, as we now load only the index from L2 SRAM instead of the complete weights. As a result, the speedup effect of weight compression becomes more noticeable as the array size increases. The speed-up of WS-CMS is less significant because the frequent L1 access greatly constrains the performance of WS dataflow.

7.5 Efficiency Analysis

Then, we compared the energy efficiency of five accelerators (measured in TOPS/W) using different array sizes. A detailed comparison on ResNets can be found in Fig. 19. It’s worth noting that the energy consumption shown in Fig. 19 does not include main memory access, which typically accounts for a significant portion of the total energy consumption. Our proposed accelerator benefits from both reduced energy consumption and enhanced performance, showing significant efficiency improvements for both WS

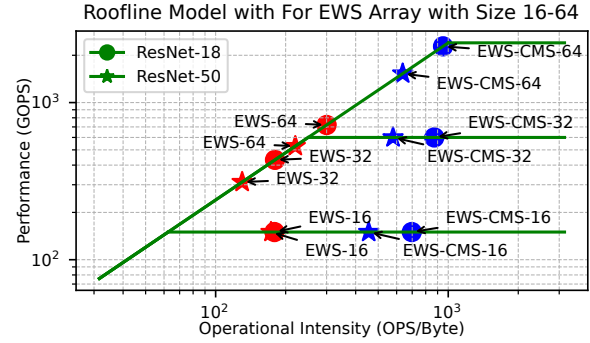


Figure 18. Roofline Model for EWS Array with different sizes

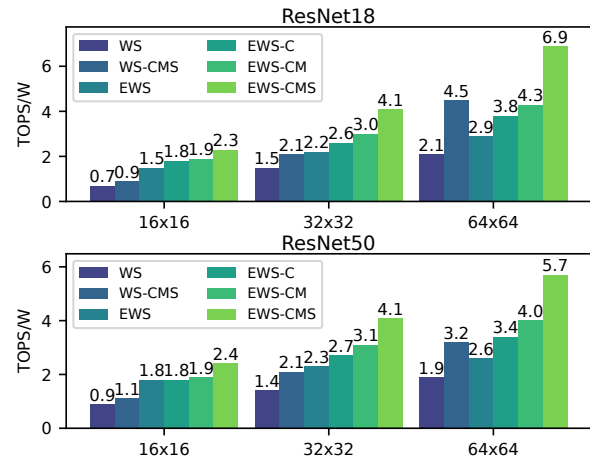


Figure 19. Energy efficiency comparison of different hardware settings on three array sizes

and EWS dataflows. Generally, as the array size increases, energy efficiency tends to improve. In comparison to the EWS baseline, our proposed EWS-CMS accelerator achieves 53.3% to 137.9% higher energy efficiency on ResNet18. Likewise, our WS-CMS accelerator achieves 28.5% to 114.2% higher energy efficiency relative to the WS baseline. It is noteworthy that the L1 power consumption is higher in the WS dataflow, which leads to a slightly smaller MVQ improvement for WS compared to EWS.

	SparTen [8]	CGNet [11]	SPOTS [30]	S2TA [21]	Ours			
	MICRO19	MICRO19	TACO22	HPCA22	MVQ-16	MVQ-32	MVQ-64	
Process(nm)	45	28	45	16/65	40			
Freq(GHz)	0.8	0.5(0.9V)	0.5	1/0.5	0.3			
SRAM Size	NA	606K+576K	1M+512K	2M+512K	2M+128KB	2M+256K		
MACs	32	576	512	2048	64	256	1024	1024(2048)
Sparse Granularity	Random	Channel-wise	Group-wise	N:M	N:M			
Sparsity	NA	60%	27%	50%	75%	75%	75%	75%(50%)
Quantization	INT8	INT8	INT16	INT8	INT8	INT8	INT8	INT8
Compression Ratio	NA	10×	3×	6.4×	22×	22×	22×	25×
Workload	AlexNet	ResNet18	VGG16	AlexNet	ResNet18	ResNet18	ResNet18	AlexNet
Dataflow	OS	WS	OS	OS	EWS			
Peak Performance(TOPS)	0.2	2.4	0.5	8/4	0.15	0.6	2.4	2.4(4.8)
Area(mm ²)	0.766	5.574	8.61	3.8/24	8.66	10.02	11.68	11.68(12.48)
Efficiency(TOPS/W)	0.68	4.5	0.47	14/1.1	2.3	4.1	6.9	4.4(3.8)
N-Efficiency(TOPS/W)	0.97	2.43	0.67	1.64/2.19	2.3	4.1	6.9	4.4(3.8)

Table 9. Comparison with Other Works. We refer to [32] to normalize energy efficiency into 40nm process.

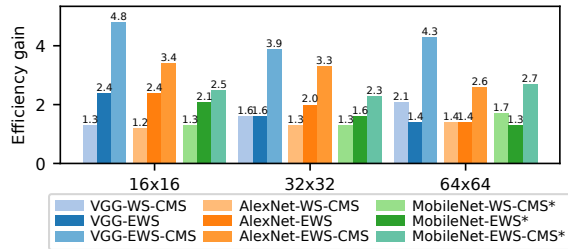


Figure 20. Energy efficiency gain compared to WS baseline on more models. * denotes pointwise convolution only.

Furthermore, the efficiency improvements for VGG16, AlexNet, and MobileNetV1 are depicted in Fig. 20. Our proposed accelerator demonstrates an average efficiency improvement 46% and 90% for WS and EWS dataflow, respectively. It is important to note that for WS/EWS dataflows, depthwise convolution requires mapping weight elements to the diagonal of the PE array. This results in the low performance of the depthwise layer as only the diagonal elements are involved in the computation. Moreover, the number of parameters in the depthwise layer is quite limited, meaning that the hardware operation bottleneck does not stem from the weight-loading process. As a result, depthwise layers don't fully utilize the advantages brought by MVQ. Therefore, we present pointwise convolution results only.

7.6 Comparison with other sparse CNN accelerators

Our MVQ is compared with a series of sparse CNN accelerators, including SparTen [8], CGNet [11], SPOTS [30], and S2TA [21]. Additionally, we have normalized the energy efficiency for a 40 nm process to ensure a fair comparison. Compared to existing works, our design greatly reduces the data access cost with MVQ which achieves a very high compression ratio. As depicted in Tab. 9, compared to S2TA [21] which reports the highest efficiency and the lowest power

consumption, our MVQ achieves 73% higher energy efficiency on AlexNet. This highlights the efficiency of our design.

8 Conclusion

This paper proposes a highly efficient accelerator with a Masked Vector Quantization (MVQ) compression method. At the algorithm level, to address the issue that important weights are often forced to align with unimportant ones, N:M pruning has been performed within each subvector to remove the unimportant weights. Subsequently, the mask k-means algorithm has been applied to prevent pruned weights from interfering with the vector clustering process. As a result, our method significantly reduces the vector clustering error compared with existing approaches. At the architecture level, we implement an area- and energy-efficient accelerator based on the EWS dataflow. Employing an index-based weight-loading unit and a sparsity-aware systolic array, our accelerator fully realizes the benefits brought by MVQ.

Algorithm experiments on various models demonstrate that our approach reaches higher accuracy at the same compression ratios and reduces FLOPs. In 40nm ASIC post-synthesis evaluation, our proposed MVQ-based accelerator can boost energy efficiency by 2.3× and cut the array size by 55% compared to the base EWS accelerator. This has also led to a superior performance of our accelerator against prior arts under energy efficiency (1.73×).

Acknowledgments

We thank our shepherd, Macro Donato, for his ongoing support and guidance during the revision process. We also thank the anonymous reviewers for their constructive feedback for improving the work. This work was supported by the National Natural Science Foundation of China under Grant 62274142 and the Shenzhen Science and Technology Program under Grant KJZD20230923115213027.

References

- [1] Liang-Chieh Chen. Rethinking atrous convolution for semantic image segmentation. *arXiv preprint arXiv:1706.05587*, 2017.
- [2] Weihan Chen, Peisong Wang, and Jian Cheng. Towards convolutional neural networks compression via global&progressive product quantization. In *BMVC*, 2020.
- [3] Yu-Hsin Chen, Tushar Krishna, Joel S Emer, and Vivienne Sze. Eyeriss: An energy-efficient reconfigurable accelerator for deep convolutional neural networks. *IEEE journal of solid-state circuits*, 52(1):127–138, 2016.
- [4] Minsik Cho, Keivan A. Vahid, Saurabh Adya, and Mohammad Rastegari. Dkm: Differentiable k-means clustering layer for neural network compression, 2022.
- [5] Steven K Esser, Jeffrey L McKinstry, Deepika Bablani, Rathinakumar Appuswamy, and Dharmendra S Modha. Learned step size quantization. *arXiv preprint arXiv:1902.08153*, 2019.
- [6] Mark Everingham, Luc Van Gool, Christopher KI Williams, John Winn, and Andrew Zisserman. The pascal visual object classes (voc) challenge. *International journal of computer vision*, 88:303–338, 2010.
- [7] Hasan Genc, Seah Kim, Alon Amid, Ameer Haj-Ali, Vighnesh Iyer, Pranav Prakash, Jerry Zhao, Daniel Grubb, Harrison Liew, Howard Mao, et al. Gemmini: Enabling systematic deep-learning architecture evaluation via full-stack integration. In *2021 58th ACM/IEEE Design Automation Conference (DAC)*, pages 769–774. IEEE, 2021.
- [8] Ashish Gondimalla, Noah Chesnut, Mithuna Thottethodi, and TN Vijaykumar. Sparten: A sparse tensor accelerator for convolutional neural networks. In *Proceedings of the 52nd Annual IEEE/ACM International Symposium on Microarchitecture*, pages 151–165, 2019.
- [9] Yunchao Gong, Liu Liu, Ming Yang, and Lubimir Bourdev. Compressing deep convolutional networks using vector quantization. *arXiv preprint arXiv:1412.6115*, 2014.
- [10] Song Han, Huizi Mao, and William J Dally. Deep compression: Compressing deep neural networks with pruning, trained quantization and Huffman coding. *arXiv preprint arXiv:1510.00149*, 2015.
- [11] Weizhe Hua, Yuan Zhou, Christopher De Sa, Zhiru Zhang, and G Edward Suh. Boosting the performance of cnn accelerators with dynamic fine-grained channel gating. In *Proceedings of the 52nd Annual IEEE/ACM international symposium on microarchitecture*, pages 139–150, 2019.
- [12] Dongseok Im, Gwangtae Park, Zhiyong Li, Junha Ryu, and Hoi-Jun Yoo. Sibia: Signed bit-slice architecture for dense dnn acceleration with slice-level sparsity exploitation. In *2023 IEEE International Symposium on High-Performance Computer Architecture (HPCA)*, pages 69–80. IEEE, 2023.
- [13] Herve Jegou, Matthijs Douze, and Cordelia Schmid. Product quantization for nearest neighbor search. *IEEE transactions on pattern analysis and machine intelligence*, 33(1):117–128, 2010.
- [14] Norman P Jouppi, Cliff Young, Nishant Patil, David Patterson, Gaurav Agrawal, Raminder Bajwa, Sarah Bates, Suresh Bhatia, Nan Boden, Al Borchers, et al. In-datacenter performance analysis of a tensor processing unit. In *Proceedings of the 44th annual international symposium on computer architecture*, pages 1–12, 2017.
- [15] Diederik P Kingma and Jimmy Ba. Adam: A method for stochastic optimization. *arXiv preprint arXiv:1412.6980*, 2014.
- [16] Andrey Kuzmin, Markus Nagel, Mart van Baalen, Arash Behboodi, and Tijmen Blankevoort. Pruning vs quantization: Which is better?, 2023.
- [17] Heng Lee, Yi-Heng Wu, Yu-Sheng Lin, and Shao-Yi Chien. Convolutional neural network accelerator with vector quantization. In *2019 IEEE International Symposium on Circuits and Systems (ISCAS)*, pages 1–5. IEEE, 2019.
- [18] Hao Li, Asim Kadav, Igor Durdanovic, Hanan Samet, and Hans Peter Graf. Pruning filters for efficient convnets. *arXiv preprint arXiv:1608.08710*, 2016.
- [19] Tsung-Yi Lin, Michael Maire, Serge Belongie, James Hays, Pietro Perona, Deva Ramanan, Piotr Dollár, and C Lawrence Zitnick. Microsoft coco: Common objects in context. In *Computer Vision—ECCV 2014: 13th European Conference, Zurich, Switzerland, September 6–12, 2014, Proceedings, Part V 13*, pages 740–755. Springer, 2014.
- [20] Zhi-Gang Liu, Paul N Whatmough, and Matthew Mattina. Systolic tensor array: An efficient structured-sparse gemm accelerator for mobile cnn inference. *IEEE Computer Architecture Letters*, 19(1):34–37, 2020.
- [21] Zhi-Gang Liu, Paul N Whatmough, Yuhao Zhu, and Matthew Mattina. S2ta: Exploiting structured sparsity for energy-efficient mobile cnn acceleration. In *2022 IEEE International Symposium on High-Performance Computer Architecture (HPCA)*, pages 573–586. IEEE, 2022.
- [22] Christos Louizos, Max Welling, and Diederik P Kingma. Learning sparse neural networks through l_0 regularization. *arXiv preprint arXiv:1712.01312*, 2017.
- [23] Julieta Martinez, Jashan Shewakramani, Ting Wei Liu, Ioan Andrei Barsan, Wenyuan Zeng, and Raquel Urtasun. Permute, quantize, and fine-tune: Efficient compression of neural networks. In *Proceedings of the IEEE/CVF Conference on Computer Vision and Pattern Recognition (CVPR)*, pages 15699–15708, June 2021.
- [24] Asit Mishra, Jorge Albericio Latorre, Jeff Pool, Darko Stosic, Dusan Stosic, Ganesh Venkatesh, Chong Yu, and Paulius Micikevicius. Accelerating sparse deep neural networks. *arXiv preprint arXiv:2104.08378*, 2021.
- [25] Pavlo Molchanov, Arun Mallya, Stephen Tyree, Iuri Frosio, and Jan Kautz. Importance estimation for neural network pruning. In *Proceedings of the IEEE/CVF conference on computer vision and pattern recognition*, pages 11264–11272, 2019.
- [26] Antonio Pullini, Davide Rossi, Igor Loi, Giuseppe Tagliavini, and Luca Benini. Mr. wolf: An energy-precision scalable parallel ultra low power soc for iot edge processing. *IEEE Journal of Solid-State Circuits*, 54(7):1970–1981, 2019.
- [27] Alex Renda, Jonathan Frankle, and Michael Carbin. Comparing rewinding and fine-tuning in neural network pruning. *arXiv preprint arXiv:2003.02389*, 2020.
- [28] Davide Rossi, Francesco Conti, Manuel Eggiman, Stefan Mach, Alfio Di Mauro, Marco Guermandi, Giuseppe Tagliavini, Antonio Pullini, Igor Loi, Jie Chen, et al. 4.4 a 1.3 tops/w@ 32gops fully integrated 10-core soc for iot end-nodes with 1.7 μ w cognitive wake-up from mram-based state-retentive sleep mode. In *2021 IEEE International Solid-State Circuits Conference (ISSCC)*, volume 64, pages 60–62. IEEE, 2021.
- [29] Jaehyeong Sim, Somin Lee, and Lee-Sup Kim. An energy-efficient deep convolutional neural network inference processor with enhanced output stationary dataflow in 65-nm cmos. *IEEE Transactions on Very Large Scale Integration (VLSI) Systems*, 28(1):87–100, 2019.
- [30] Mohammadreza Soltaniyeh, Richard P Martin, and Santosh Nagarakatte. An accelerator for sparse convolutional neural networks leveraging systolic general matrix-matrix multiplication. *ACM Transactions on Architecture and Code Optimization (TACO)*, 19(3):1–26, 2022.
- [31] Sanghyun Son, Seungjun Nah, and Kyoung Mu Lee. Clustering convolutional kernels to compress deep neural networks. In *Proceedings of the European conference on computer vision (ECCV)*, pages 216–232, 2018.
- [32] Aaron Stillmaker and Bevan Baas. Scaling equations for the accurate prediction of cmos device performance from 180 nm to 7 nm. *Integration*, 58:74–81, 2017.
- [33] Pierre Stock, Armand Joulin, Rémi Gribonval, Benjamin Graham, and Hervé Jégou. And the bit goes down: Revisiting the quantization of neural networks. *arXiv preprint arXiv:1907.05686*, 2019.
- [34] Wei Sun, Aojun Zhou, Sander Stuijk, Rob Wijnhoven, Andrew O Nelson, Henk Corporaal, et al. Dominosearch: Find layer-wise fine-grained n: M sparse schemes from dense neural networks. *Advances in neural*

- information processing systems*, 34:20721–20732, 2021.
- [35] Chengxuan Wang, Zongsheng Wang, Shuaiting Li, Yuanming Zhang, Haibin Shen, and Kejie Huang. Ews: An energy-efficient cnn accelerator with enhanced weight stationary dataflow. *IEEE Transactions on Circuits and Systems II: Express Briefs*, 2024.
- [36] Jiayang Wu, Cong Leng, Yuhang Wang, Qinghao Hu, and Jian Cheng. Quantized convolutional neural networks for mobile devices. In *Proceedings of the IEEE conference on computer vision and pattern recognition*, pages 4820–4828, 2016.
- [37] Yi-Heng Wu, Heng Lee, Yu Sheng Lin, and Shao-Yi Chien. Accelerator design for vector quantized convolutional neural network. In *2019 IEEE International Conference on Artificial Intelligence Circuits and Systems (AICAS)*, pages 46–50. IEEE, 2019.
- [38] Aojun Zhou, Yukun Ma, Junnan Zhu, Jianbo Liu, Zhijie Zhang, Kun Yuan, Wenxiu Sun, and Hongsheng Li. Learning n: m fine-grained structured sparse neural networks from scratch. *arXiv preprint arXiv:2102.04010*, 2021.